Journal of Innovative Optical Health Sciences
Vol. 3, No. 4 (2010) 307–313
© World Scientific Publishing Company
DOI: 10.1142/S1793545810001167

World Scientific
www.worldscientific.com

J. Innov. Opt. Health Sci. 2010.03:307-313. Downloaded from www.worldscientific.com
by HUAZHONG UNIVERSITY OF SCIENCE AND TECHNOLOGY on 10/24/18. Re-use and distribution is strictly not permitted, except for Open Access articles.

LABEL-FREE 3D OPTICAL MICROANGIOGRAPHY IMAGING OF FUNCTIONAL VASA NERVORUM AND PERIPHERAL MICROVASCULAR TREE IN THE HIND LIMB OF DIABETIC MICE

YALI JIA*, THOMAS K. BAUMANN*,† and RUIKANG K. WANG*,‡,§
*Department of Biomedical Engineering
Oregon Health & Science University
3303 SW Bond Avenue, Portland, Oregon 97239, USA
†Departments of Neurological Surgery, Physiology and Pharmacology
Oregon Health & Science University
3181 SW Sam Jackson Park Road
Portland, Oregon 97239, USA
‡Department of Bioengineering, University of Washington
3720, 15th Ave NE, Seattle, Washington 98195, USA
§wangrk@u.washington.edu

Diabetic neuropathy (DN) is, at least in part, associated with the functional attenuation of vasa nervorum, the microvascular structure of peripheral nerves. Microvascular imaging options for vasa nervorum still remain limited. In this work, optical microangiography (OMAG), a volumetric, label-free imaging technique, is utilized for characterizing, with high resolution, blood perfusion of peripheral nerve in diabetic mice. We demonstrate that OMAG is able to visualize the structure of microvasculature and to quantify the changes of dynamic blood flow and vessel diameters during administration of vessel stimulant in both diabetic and normal mice. The results indicate the potential of OMAG to assess the blood supply of nerve involved in the pathology and treatment of DN.

Keywords: Vasa nervorum; microcirculation; peripheral nerve; diabetes; optical microangiography.

1. Introduction

Diabetic neuropathy (DN) is the most common complication of diabetes mellitus, affecting up to 60% of diabetic patients.[1] Loss of sensation in the feet, the most frequent manifestation of diabetic neuropathy, frequently leads to foot ulcers and may progress onto amputation of the limb.[2] Despite a continuous increase in the incidence of diabetes mellitus and DN, the pathogenic basis underlying DN has remained uncertain, and current treatments have yet to effectively treat DN.[3] It has been noted in multiple previous reports that experimental DN is characterized by reduced microcirculation in peripheral nerves resulting from the decrease in blood flow through the vasa nervorum, the microvessels that provide blood supply to peripheral nerves and thus the restoration of nerve blood flow supply may mitigate neuropathy despite persistent diabetes.[4]

Accordingly, to investigate the association between the changes of blood flow in the vasa

J. Innov. Opt. Health Sci. 2010.03:307-313. Downloaded from www.worldscientific.com
by HUAZHONG UNIVERSITY OF SCIENCE AND TECHNOLOGY on 10/24/18. Re-use and distribution is strictly not permitted, except for Open Access articles.

nervorum and DN, and to further evaluate the treatments on DN by administrating the factors increasing the nerve perfusion, a non-invasive technique for assessing blood perfusion in vasa nervorum (visualizing and quantifying blood circulation) would be of great value. Currently, the common research methods to study the vascular supply of peripheral nerves in diabetic animal models are fluorescent imaging of vascular architecture[5] and laser Doppler imaging of blood flow.[6–8] Although they have made significant contributions to our understanding of vascular pathology associated with DN, their important limitations still remain. Fluorescent imaging cannot provide dynamic images on the same animals due to its invasiveness, and laser Doppler perfusion imaging only produces the relative values of blood flow and is only valid for the perfusion on the tissue surface. In this paper, we demonstrate a potential method for functional imaging of blood perfusion of vasa nervorum *in vivo*.

Recently, optical coherence tomography (OCT) has been widely used to detect the pathological changes of tissues[9–12] in preclinical models in order to guide clinical diagnosis. Optical microangiography (OMAG)[13] as a functional extension of OCT,[14,15] is a volumetric, label-free imaging technique that is recently developed in our group for imaging dynamic blood perfusion, especially for diagnosing pathological changes of blood vessels. The imaging is achieved by separating the signals backscattered by moving blood cells from those originated from tissue microstructures. Because its imaging contrast is based on endogenous light scattering from moving blood cells within biological tissue, no exogenous contrast agents are required for imaging. Its imaging depth is up to 2 mm in biological tissue. Wang *et al.* recently demonstrated mouse brain imaging through both intact scalp and skull.[16] This non-invasive feature is highly desirable for functional or chronic studies. Its current spatial resolution (lateral resolution: 16 μm, axial resolution: 8 μm) allows us to resolve microcirculations and even capillaries. Combined with phase-resolved method, now the second version of OMAG could extract flow velocities from flow signals and produce the flow map and velocity map simultaneously.[17] In this paper, in an attempt to show the potential of OMAG to visualize the dysfunctional microcirculation after DN and monitor the regulation on blood flow after treatments, we used OMAG to non-invasively monitor the changes of blood flow in both diabetic and normal mice with topical application to the skin of a sensory stimulant chemical, menthol.

2. Methods

The configuration and operating principles of OMAG system can be found elsewhere.[17] Briefly, the system used in this study employed a broadband infrared superluminescent diode with a central wavelength of 1.3 μm. The spectral interferogram formed by lights between the sample and reference arms was sent to a home-built high-speed spectrometer that employed a line scan infrared InGaAs detector to achieve an imaging speed of 20 frames per second (fps) with 1,000 A scans (axial scans) in each B scan (lateral direction). The system has the imaging resolution of $16 \times 16 \times 8\,\mu m^3$ in the x–y–z direction, and an imaging depth of ~3 mm in air.

We examined both diabetic mice (using the $Ins2^{Akita/+}$ mutant model of Type 1 diabetes with neonatal onset) and their non-diabetic (normal) siblings. The "Akita" mouse carries a C96Y mis-sense mutation in the proinsulin gene. This mutation is identical to the one recently discovered in boys with neonatal onset Type 1 diabetes. The autosomal dominant inheritance pattern in both mouse and human makes this mouse mutant a valuable model for study of complications associated with permanent diabetes.[18]

The experimental protocol was in compliance with the federal guidelines for care and handling of small rodents and approved by the Institutional Animal Care and Use Committee. Before functional optical imaging, the right hind limb of mice was shaved and depilated. In order to further improve the resolution of the images, a small patch was excised to form a small ($\sim 3 \times 3\,mm^2$) window over the subcutaneous tissues being imaged. During the imaging, the animal was immobilized in a custom-made stereotaxic stage and was lightly anesthetized with isoflurane (0.2 L/min O_2, 0.8 L/min air). The body temperature was kept between 35.5–36.5°C by use of a warming blanket, and monitored by a rectal thermal probe throughout the experiment. Saphenous nerve, a representative peripheral nerve, was chosen as imaging site due to its superficial location and was positioned under the scanning probe. The imaging area was kept moist under a piece of plastic foil. Before administrating the sensory irritant, a control C scan (3D) and the repeated B scans over one minute duration were acquired as the baseline

J. Innov. Opt. Health Sci. 2010.03:307-313. Downloaded from www.worldscientific.com
by HUAZHONG UNIVERSITY OF SCIENCE AND TECHNOLOGY on 10/24/18. Re-use and distribution is strictly not permitted, except for Open Access articles.

for later comparison. The imaging sites of C-scan and B-scan are shown by solid line box and dashed line, respectively, in Fig. 1(d). Then a small cotton ball was dipped in 40% menthol solution in ethanol and gently loaded on the lower end of hind limb. Once menthol was administered, B-scan was initiated and repeated for six minutes. Then final C-scan recorded the perfusion with stimulation on the same site as control. The total imaging acquisition time in this process was 8 minutes.

3. Results

The original raw data cube (spectral interferograms) was first processed frame by frame, and then the resulting images — including structural, flow and velocity images — were combined to produce a 3D volumetric visualization of the scanned tissue volume. The results for a typical limb tissue volume of $2.5 \times 2.5 \times 2.0\,\text{mm}^3$ are given in Fig. 1. Figure 1(a) is a volumetric visualization rendered by merging the microstructural 3D image with the corresponding 3D image of functional blood flows, where the precise location of blood flow can be identified together with the microstructures of the tissue. In this image, a cut-away view is utilized to show how the blood vessels are distributed in the tissue volume. Figure 1(b) shows the volumetric network of blood vessels within the scanned tissue volume, where the bundle of vessels indicated in a rectangle box was vasa nervorum running longitudinally in the saphenous nerve along with the femoral artery and vein. It can also be noted that the longitudinal vessels in the epineurium are connected with one another by transverse anastomoses pointed out by white arrows. To show in detail the blood vessel networks, the maximum projection approach was used to obtain x–y projection network in Fig. 1(c), in which numerous strips on the formal artery caused by the heart beat were clearly

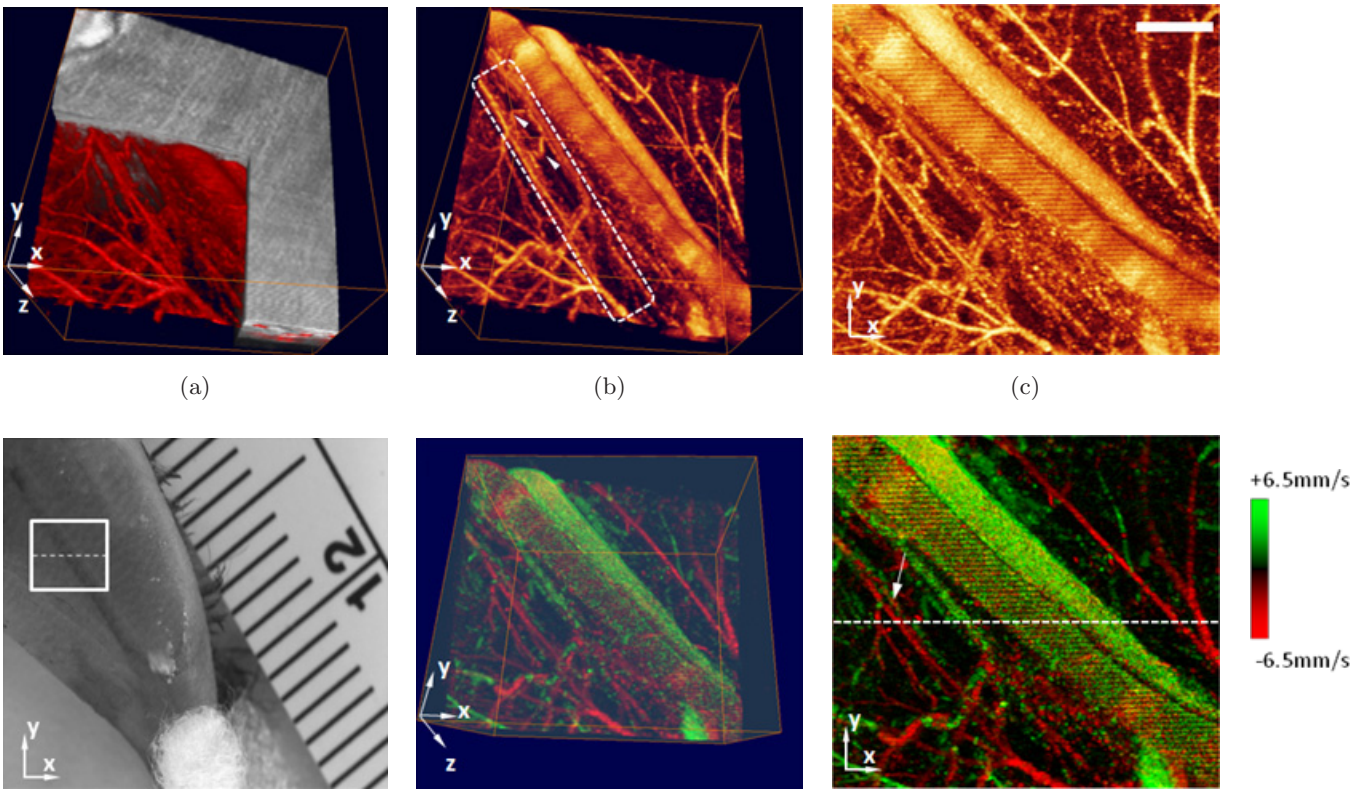

Fig. 1. *In vivo* 3D OMAG imaging of the hind limb of mouse over an area covering a part of saphenous nerve indicated by white box in photograph (d). (a) The volumetric visualization was rendered by merging the 3D microstructural image with the 3D blood flow image. (b) The 3D signals of blood flow in vasa nervorum and vessels around it. (e) The corresponding image of velocities in 3D vascular network. (c) and (f) are the maximum projection view (x–y) of (b) and (e). The green color in (e) and (f) represents that the blood moves towards the incident probe beam, and otherwise the red color. Scale Bar = 500 μm [applies to (c) and (f)].

J. Innov. Opt. Health Sci. 2010.03:307-313. Downloaded from www.worldscientific.com
by HUAZHONG UNIVERSITY OF SCIENCE AND TECHNOLOGY on 10/24/18. Re-use and distribution is strictly not permitted, except for Open Access articles.

shown. The corresponding velocity information is shown in Figs. 1(e) and 1(f). The directional flow information was coded with colors, where the green color means the blood moves toward the incident beam direction and otherwise the red color. In the light of this, the vessels of varying flow direction are demonstrable within the microvascular architecture of the peripheral nerve.

Previous studies[19] reported that the individual vascular cord in vasa nervorum consists of nutrient arterioles, venules and capillary plexus. Although capillary plexus cannot be clearly delineated in our OMAG flow and velocity images due to the close positions between the arteriole and the venule, the cloudy signals backscattered from capillary are distributed in the single vessel cord indicated by an arrow. Here, OMAG velocity images provide a potential tool to quantify blood perfusion within the microcirculation tissue beds in vasa nervorum *in vivo*.

Next, shown in Fig. 2 are the representative results from a single B-scan (frame) of a mouse hind limb, the position of which is indicated by the white dashed line in Fig. 1(f). Figure 2(a) is the OMAG structural image, where the important histological structures, including the femoral artery and vein, the nerve bundle, are shown. Figure 2(b) shows the corresponding image of localized blood flow that

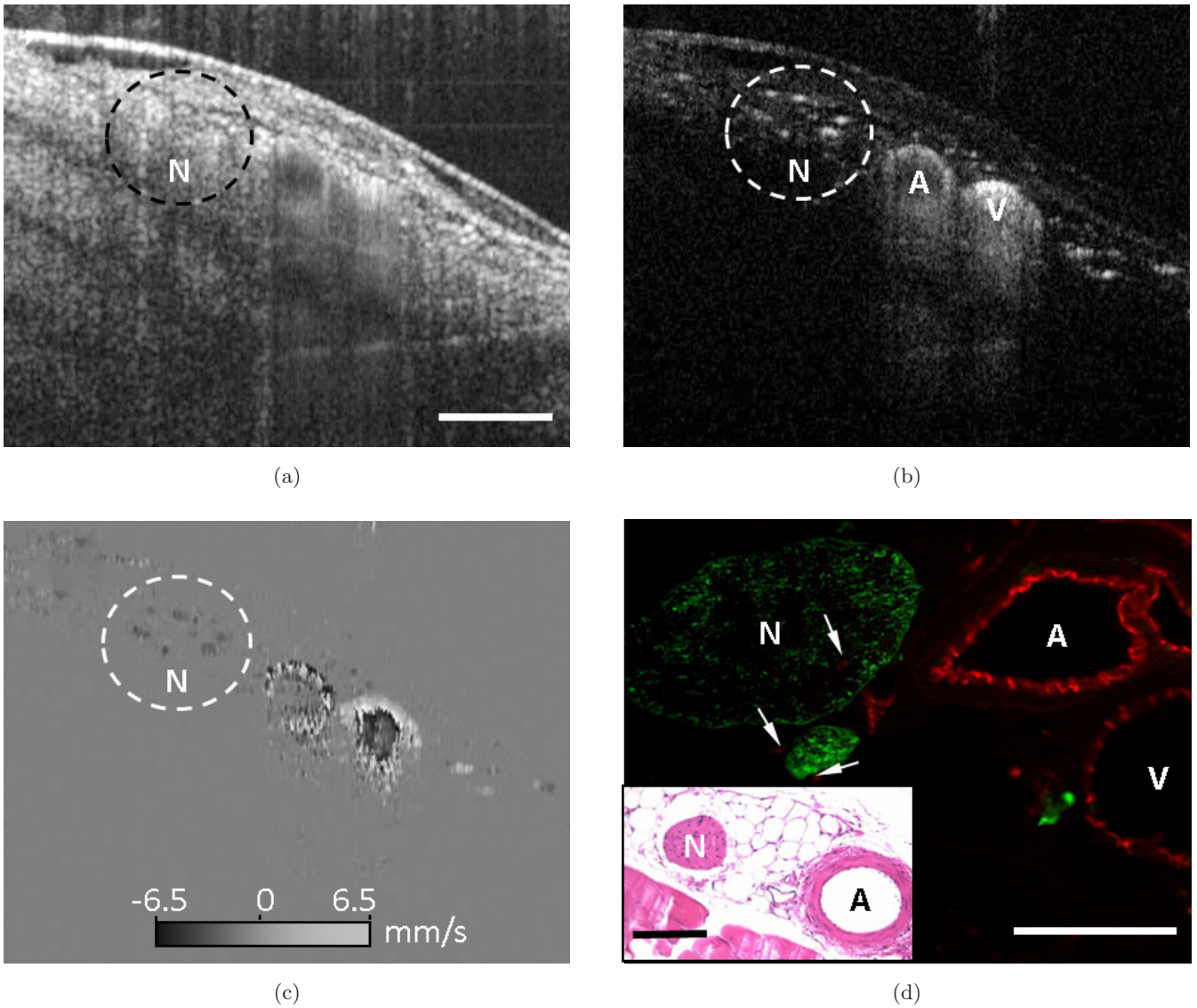

Fig. 2. Comparison between *in vivo* OMAG (B-scan) and histological imaging of the vasa nervorum within peripheral nerve bundle of mice. Shown are (a) the OMAG structural image, (b) the corresponding OMAG flow image, (c) OMAG velocity image, and (d) stained fluorescent and histology images. N, nerve; A, artery; V, vein. Bar = 500 μm.

J. Innov. Opt. Health Sci. 2010.03:307-313. Downloaded from www.worldscientific.com
by HUAZHONG UNIVERSITY OF SCIENCE AND TECHNOLOGY on 10/24/18. Re-use and distribution is strictly not permitted, except for Open Access articles.

permeates this cross-section in Fig. 2(a). The flow velocity information along the light beam direction extracted from Fig. 2(b) is given in Fig. 2(c). As expected, the flow velocity in the microcirculation at a depth of ∼1.5 mm within the vasa nervorum is imaged by OMAG, which is circled by dashed line. As a comparison, in Fig. 2(d), a cross-section of mouse hind leg tissue immunostained is used to show the position of the blood vessel in the vicinity of the saphenous nerve. Saphenous nerve and its branches detected with a myelin basic protein antibody are shown in green. Femoral artery and vein detected with an antibody to CD31 are the large blood vessels with the lumen outlined in red. The endoneurial blood vessels belonging to the vasa nervorum of the saphenous nerve and the blood vessels belonging to the vasa nervori of the nerve branches are pointed by white arrows. A traditional H&E staining image in the left corner of Fig. 2(d) also shows the location of saphenous nerve and artery, but the endoneurial blood vessels are not easily distinguishable.

In addition to volumetric visualization of microcirculation within the vasa nervorum, the OMAG system enables us, by non-invasive means, to quantitatively examine the dynamic parameters of localized blood flow around or within nerve bundles, for example, the inner diameter of the vessel and the localized flow velocity and blood flow rate. The quantitative time courses of mean flow velocity with Doppler angle correction in the representative arteriole with the same size in both diabetic and

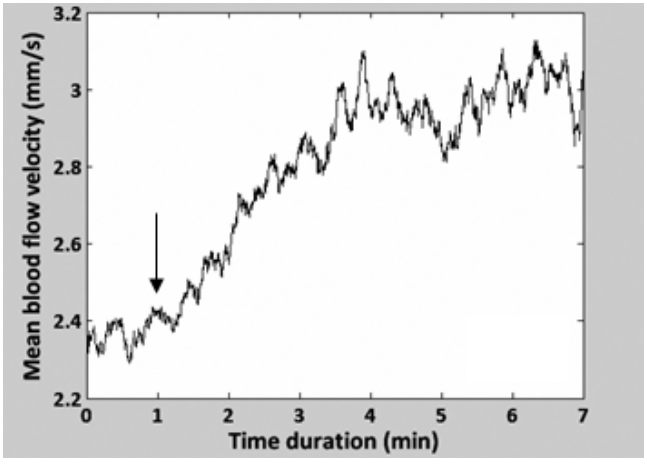

(a)

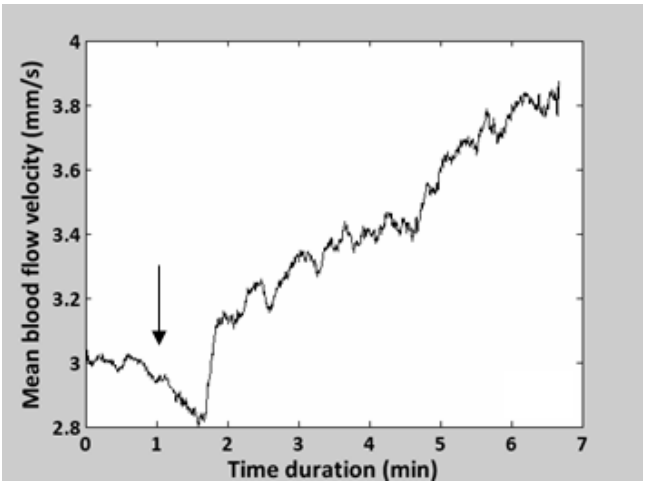

(b)

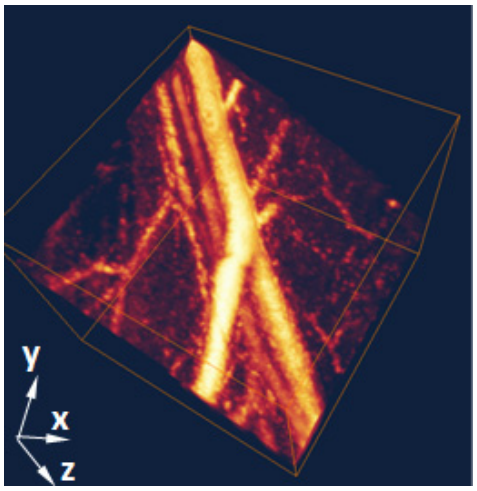

(c)

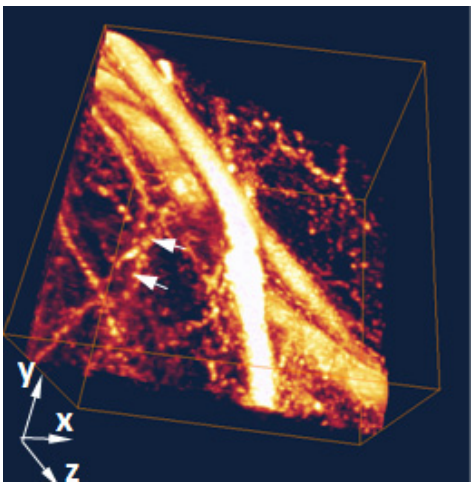

(d)

Fig. 3. *In vivo* characterization of the dynamic changes of blood flow velocity in the representative arterioles in (a) diabetic and (b) normal mice before and after chemical stimulation. Vasodilation in vasa nervorum is also shown by comparing 3D OMAG images between (c) the baseline and (d) end point of stimulation in the diabetic animal.

J. Innov. Opt. Health Sci. 2010.03:307-313. Downloaded from www.worldscientific.com
by HUAZHONG UNIVERSITY OF SCIENCE AND TECHNOLOGY on 10/24/18. Re-use and distribution is strictly not permitted, except for Open Access articles.

normal mice before and after the administration of the sensory irritant, menthol, are presented in Figs. 3(a) and 3(b), respectively. The starting time point of stimulation is indicated by black arrows. It is noted that before the administration of this vessel stimulant (baseline), the diabetic animal is easily distinguished from the normal one due to the lower blood flow velocity. After topical application of 40% menthol to the skin at a location 3 mm distal to the skin window, the blood flow in a single vessel of vasa nervorum was accelerated immediately and reached the maximum value (∼3.2 mm/s) within a few minutes in the diabetic mouse. Whereas the blood flow in a normal mouse first dropped to 80% of baseline, which was probably caused by the normal sensitivity of sensory nerve fibers to skin cooling by menthol in ethanol solution, it then continuously increased without reaching the maximum within the imaging time window, possibly due to the proper mechanical properties of vessel walls. Compared to a normal mouse, the vascular reaction on the temperature change was retarded in diabetic mouse, and the time duration of response to the irritant stimulus was short, due to the vascular malfunction involved in the DN. Accompanying the increase of blood flow velocity, in both diabetic and normal mice, the inner diameters of vessels are also increased. This was determined by comparing the two OMAG flow images at the beginning of the experiment (baseline) and the end point (7th minute). An example from a diabetic animal is presented in Figs. 3(c) and 3(d). The vasodilation is clearly indicated by white arrows in Fig. 3(d).

4. Conclusion

We have successfully demonstrated the potential use of OMAG for *in vivo* 3D visualization of microcirculation within vasa nervorum in a peripheral nerve. By regulating the blood flow in the nerve, we also demonstrated that OMAG is able to directly examine the dynamic microcirculatory parameters. In future, a simple combination of OMAG and neurophysiological methods should permit detailed evaluation of the microcirculation in the nerve and enable determination of the effects of vascular-related pharmacological inventions on DN.

Acknowledgment

This work was supported in part by research grants from the National Institutes of Health (R01HL093140, R01EB009682, and R01DC010201) (RKW), and the American Heart Association (0855733G) (RKW), and the National Institute of Diabetes and Digestive and Kidney Diseases (5 U24 DK076169-04, Pilot and Feasibility Study 09MCG81) (TKB).

References

1. J. Partanen, L. Niskanen, J. Lehtinen, E. Mervaala, O. Siitonen, M. Uusitupa, "Natural history of peripheral neuropathy in patients with non-insulin-dependent diabetes mellitus," *N. Engl. J. Med.* **333**(2), 89–94 (1995).
2. G. E. Reiber, E. J. Boyko, D. G. Smith, "Lower extremity foot ulcers and amputations in diabetes," in *Diabetes in America*, M. I. Harris, C. C. Cowie, M. P. Stern, E. J. Boyko, G. E. Reiber, P. H. Bennett (eds.), pp. 409–427, National Institute of Diabetes and Digestive and Kidney Diseases, Washington, DC (1995).
3. Z. Simmons, E. L. Feldman, "Update on diabetic neuropathy," *Curr. Opin. Neurol.* **15**(5), 595–603 (2002).
4. K. F. Kusano, K. L. Allendoerfer, W. Munger, R. Pola, M. Bosch-Marce, R. Kirchmair, Y.-S. Yoon, C. Curry, M. Silver, M. Kearney, T. Asahara, D. W. Losordo, "Sonic hedgehog induces arteriogenesis in diabetic vasa nervorum and restores function in diabetic neuropathy," *Arterioscler. Thromb. Vasc. Biol.* **24**(11), 2102–2107 (2004).
5. P. Schratzberger, D. H. Walter, K. Rittig, F. H. Bahlmann, R. Pola, C. Curry, M. Silver, J. G. Krainin, D. H. Weinberg, A. H. Ropper, J. M. Isner, "Reversal of experimental diabetic neuropathy by VEGF gene transfer," *J. Clin. Invest.* **107**(9), 1083–1092 (2001).
6. I. Rundquist, Q. R. Smith, M. E. Michel, P. Ask, P. A. Oberg, S. I. Rapoport, "Sciatic nerve blood flow measured by laser Doppler flowmetry and [14C]iodoantipyrine," *Am. J. Physiol. Heart Circ. Physiol.* **248**(3), H311–317 (1985).
7. D. W. Zochodne, P. A. Low, "Adrenergic control of nerve blood flow," *Exp. Neurol.* **109**(3), 300–307 (1990).
8. G. J. Biessels, A. Kamal, G. M. Ramakers, I. J. Urban, B. M. Spruijt, D. W. Erkelens, W. H. Gispen, "Place learning and hippocampal synaptic plasticity in streptozotocin-induced diabetic rats," *Diabetes* **45**(9), 1259–1266 (1996).
9. M. Ruggeri, H. Wehbe, G. Tsechpenakis, S. Jiao, M. E. Jockovich, C. Cebulla, E. Hernandez, T. G. Murray, C. A. Puliafito, "Quantitative evaluation of retinal tumor volume in mouse model of retinoblastoma by using ultra high-resolution

optical coherence tomography," *J. Innovat. Opt. Health Sci.* **1**(1), 17–28 (2008).
10. Z. J. Yuan, H. G. Ren, W. Waltzer, J. Kim, J. X. Liu, K. M. Jia, H. K. Xie, Y. T. Pan, "Optical coherence tomography for bladder cancer diagnosis: From animal study to clinical diagnosis," *J. Innovat. Opt. Health Sci.* **1**(1), 125–140 (2008).
11. E. Borisova, E. Carstea, L. Cristescu, E. Pavlova, N. Hadjiolov, P. Troyanova, L. Avramov, "Light-induced fluorescence spectroscopy and optical coherence tomography of basal cell carcinoma," *J. Innovat. Opt. Health Sci.* **2**(3), 261–268 (2009).
12. M. Todorovic, S. L. Jiao, G. Stoica, L. H. Wang, "Preliminary study on skin cancer detection in sencar mice using Mueller optical coherence tomography," *J. Innovat. Opt. Health Sci.* **2**(3), 289–294 (2009).
13. R. K. Wang, S. L. Jacques, Z. Ma, S. Hurst, S. Hanson, A. Gruber, "Three-dimensional optical angiography," *Opt. Express* **15**, 4083–4097 (2007).
14. A. F. Fercher, W. Drexler, C. K. Hitzenberger, T. Lasser, "Optical coherence tomography — principles and applications," *Rep. Prog. Phys.* **66**, 239–303 (2003).
15. P. H. Tomlins, R. K. Wang, "Theory, development and applications of optical coherence tomography," *J. Phys. D: Appl. Phys.* **38**, 2519–2535 (2005).
16. R. K. Wang, S. Hurst, "Mapping of cerebrovascular blood perfusion in mice with skin and cranium intact by optical microangiography at 1300 nm wavelength," *Opt. Express* **15**(18), 11402–11412 (2007).
17. R. K. Wang, L. An, "Doppler optical microangiography for volumetric imaging of vascular perfusion *in vivo*," *Opt. Express* **17**(11), 8926–8940 (2009).
18. A. J. Barber, D. A. Antonetti, T. S. Kern, C. E. N. Reiter, R. S. Soans, J. K. Krady, S. W. Levison, T. W. Gardner, S. K. Bronson, "The Ins2Akita mouse as a model of early retinal complications in diabetes," *Inv. Ophthalmol. & Visual Sci.* **46**(6), 2210–2218 (2005).
19. G. Lundborg, P. I. Branemark, "Microvascular structure and function of the peripheral nerves: Vital microscopic studies of the tibial nerve in the rabbit," *Adv. Microcirc.* **1**(2), 66–88 (1968).

J. Innov. Opt. Health Sci. 2010.03:307-313. Downloaded from www.worldscientific.com
by HUAZHONG UNIVERSITY OF SCIENCE AND TECHNOLOGY on 10/24/18. Re-use and distribution is strictly not permitted, except for Open Access articles.